Available online at www.sciencedirect.com
ScienceDirect
Magnetic Resonance Imaging 25 (2007) 449–452
MAGNETIC RESONANCE IMAGING

Dispersion measurements using time-of-flight remote detection MRI

Josef Granwehr[a,b,*], Elad Harel[a], Christian Hilty[a], Sandra Garcia[a], Lana Chavez[a], Alex Pines[a], Pabitra N. Sen[c], Yi-Qiao Song[c]

[a]*Materials Sciences Division, Lawrence Berkeley National Laboratory and University of California at Berkeley, Berkeley, CA 94720, USA*
[b]*Sir Peter Mansfield Magnetic Resonance Center, School of Physics and Astronomy, University of Nottingham, Nottingham NG7 2RD, UK*
[c]*Schlumberger-Doll Research, One Hampshire Street, Cambridge, MA 02139, USA*

Abstract

Remote detection nuclear magnetic resonance and magnetic resonance imaging can be used to study fluid flow and dispersion in a porous medium from a purely Eulerian point of view (i.e., in a laboratory frame of reference). Information about fluid displacement is obtained on a macroscopic scale in a long-time regime, while local velocity distributions are averaged out. It is shown how these experiments can be described using the common flow propagator formalism and how experimental data can be analyzed to obtain effective porosity, flow velocity inside the porous medium, fluid dispersion and flow tracing of fluid.

Keywords: Magnetic resonance; Imaging; Remote detection; Dispersion; Flow; Time of flight

Remote detection nuclear magnetic resonance (NMR) and magnetic resonance imaging (MRI) denominate a magnetic resonance experiment where encoding and detection are spatially and temporally separated, thereby facilitating individual optimization of both [1]. During encoding, information about a sample of interest is transferred onto the longitudinal spin magnetization M_z of a fluid, which acts as a "spin sensor." This fluid is then relocated to a detector, where its M_z is read out. The sample can be a stationary porous object, the fluid itself as it passes through an object or both at the same time. Encoding is performed point by point and can comprise any pulse sequence that is able to transfer the desired information onto the spin sensor. Detection can be performed with any method or device capable of sensitively measuring the longitudinal spin magnetization of the fluid; for example, an inductive detector [1] at high magnetic field, a magnetometer [2] that allows detection time constants up to the longitudinal relaxation time T_1 of the fluid magnetization or a device that is specifically designed to record only the spin magnetization of the fluid, such as spin-exchange optical detection for hyperpolarized noble gases [3].

Since only one phase component of transverse magnetization can be encoded at a time, a two-step phase cycle is necessary to record a complex data point. Let us assume an arbitrary encoding sequence ending with a $\pi/2$ storage pulse on the fluid spins to transfer precessing transverse magnetization into longitudinal magnetization and to transfer the remaining longitudinal magnetization into transverse magnetization, which dephases until the fluid reaches the detector. Fluid magnetization immediately before the storage pulse shall be $M^+(t_1^-)=M(t_1)\exp(i\theta)$, where t_1 is the duration of the encoding sequence, $M(t_1)$ is the amplitude of transverse magnetization and θ is its phase. A $-y$ pulse stores the x component of M^+ as longitudinal magnetization, and one obtains $M_z(t_1^+)=M(t_1)\cos(\theta)$ after the storage pulse. The y component of M^+ is obtained with the storage pulse shifted by 90°. The remotely measured signal is proportional to the longitudinal magnetization M_z^R of the fluid in the detection volume. To calculate M_z^R, multiple additional factors have to be taken into account. If only a fraction $\zeta<1$ of the fluid inside the detection volume was encoded, unencoded fluid with magnetization M_0' adds a baseline to the signal, causing a peak at the center of the encoded spectrum or image in an experiment with Fourier encoding. Due to the relaxation of the fluid towards thermal equilibrium M_0, remote signals get scaled by a factor $\lambda\leq 1$. In the

* Corresponding author. Sir Peter Mansfield Magnetic Resonance Center, School of Physics and Astronomy, University of Nottingham, NG7 2RD Nottingham, UK. Tel.: +44 115 9515151x18274; fax: +44 115 9515166.
E-mail address: josef.granwehr@nottingham.ac.uk (J. Granwehr).

0730-725X/$ – see front matter © 2007 Elsevier Inc. All rights reserved.
doi:10.1016/j.mri.2006.11.011

Table 1
Phase cycle for remote NMR experiments

Step	Storage	$M_z(t_1^+)$	Weight	$M_z^R(t_1)\times$weight factor
1	$-y$	$M(t_1)\cos(\theta)$	1	$\lambda(\zeta M(t_1)\cos(\theta)+(1-\zeta)M_0')$
2	x	$M(t_1)\sin(\theta)$	i	$i\lambda(\zeta M(t_1)\sin(\theta)+(1-\zeta)M_0')$
3	y	$-M(t_1)\cos(\theta)$	-1	$\lambda(\zeta M(t_1)\cos(\theta)-(1-\zeta)M_0')$
4	$-x$	$-M(t_1)\sin(\theta)$	$-i$	$i\lambda(\zeta M(t_1)\sin(\theta)-(1-\zeta)M_0')$

The first two steps recover the complex signal and allow frequency discrimination along an encoded dimension. The subsequent two steps remove the baseline caused by the unencoded fluid in the detector. $M_0' \gg M_0$ was assumed, but the phase cycle also works if M_0 cannot be neglected. Using a weight factor for recorded data instead of cycling the detection pulse phase makes this scheme suitable not only for inductive detectors but also for any other detector capable of measuring M_z of the encoded fluid.

case of a thermally polarized fluid where $M_0' = M_0$, this adds another contribution to the baseline, while for hyperpolarized fluids with $M_0' \gg M_0$, relaxation reduces both the intensity of the baseline and the signal. Finally, one obtains

$$M_z^R(t_1) = \lambda\left(\zeta M_z\left(t_1^+\right) + (1-\zeta)M_0'\right) + (1-\lambda)M_0. \quad (1)$$

Note that for prepolarized fluids with negligible equilibrium polarization, not the time between encoding and detection but the time between inflow of the fluid into a porous medium and detection determines signal damping. For homogeneous porous media without multiple distinguishable flow paths, λ does not depend on the encoding location and is constant [4]. In contrast, with direct detection using the same coil as for encoding, the time between inflow and detection is location dependent, and a spatially dependent signal correction must be performed [5]. On the other hand, with a fluid that is Boltzmann-polarized inside the porous medium, remote detection requires signal correction, while direct detection does not.

If the flow is steady and if the flow rate is stable, the baseline does not change significantly for different encoding steps. It can be identified once and then subtracted during data processing. Another possibility is to add two more steps to the phase cycle with inverted phase of the storage pulse. This changes the sign of encoded information, while the baseline remains constant. Subtracting this second cycle from the first doubles the signal and removes the baseline (Table 1). The weighted sum of the signals from all four steps is proportional to

$$S(t_1) \propto 2\zeta\lambda M(t_1)[\cos(\theta) + i\sin(\theta)] = 2\zeta\lambda M^+\left(t_1^-\right). \quad (2)$$

If the flow is not steady, phase cycling becomes more error-prone as the fraction of the unencoded fluid in the detector varies. For rapidly fluctuating or pulsating flow, as well as for the flow of multiple immiscible phases or in the presence of bubbles, the phase cycle may fail entirely.

The inherently present fluid flow in experiments with remote detection can be studied itself by time-resolved recording of the arrival of the encoded fluid at the detector [6], requiring a detector with an active volume V_d that is smaller than the encoded fluid volume. With inductive detection using a second coil, the time of flight (TOF) of the encoded fluid can be measured stroboscopically by applying a train of detection pulses, followed by the recording of the free induction decay after each pulse. The TOF can then be correlated with an encoded property, be it an image [6], a spectrum [7] or any other quantity that can be encoded in an NMR experiment. In the case of image encoding, a series of partial images is obtained, each showing a snapshot of the location of the detected fluid during encoding. Fig. 1A shows gas flow through a porous Bentheimer sandstone using hyperpolarized ^{129}Xe as the target nucleus. This experiment is equivalent to the established experiment of measuring a breakthrough curve of a tracer injected at one end of a column or porous sample to study hydrodynamic dispersion [8]. The magnetic resonance version's advantage is that encoding is much more flexible. Using field gradients, the fluid inside the sample can be addressed noninvasively with spatial selectivity, allowing one to extract the dispersion curve individually for arbitrary "injection" locations. In addition, spins are truly ideal tracers (i.e., manipulating them does not affect the liquid's properties). On the downside, the magnetic resonance experiment requires the detection to be performed on a timescale on the order of T_1 of the sensor spins. Admixing a component with a long T_1 to the fluid of interest can extend the available timescale, but may also alter the fluid properties such as viscosity or density, and the diffusivity may be changed because a different species is observed.

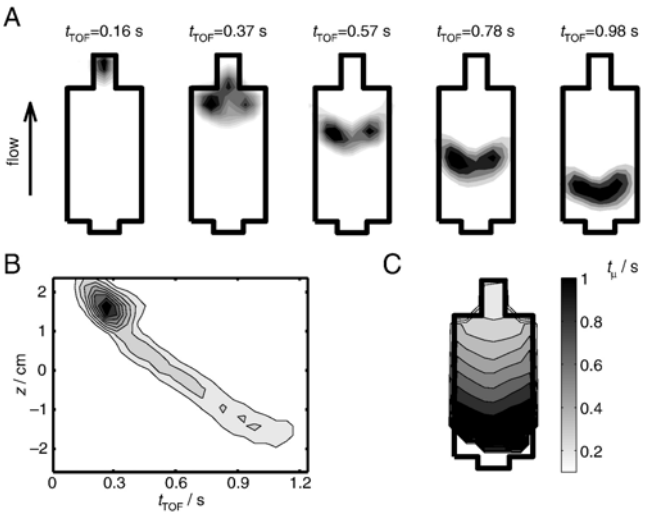

Fig. 1. Studying flow in a Bentheimer sandstone with remote detection MRI [6]. For analysis, a slice along the axis of the cylindrical sample was used from a data set that was recorded with three-dimensional phase encoding. (A) Visualizing fluid displacement by plotting the fluid location at time t_{TOF} before it reaches the detector. The sample profile and the inlet and outlet are outlined by a black line. (B) Plot of the t_{TOF} for the fluid that was tagged along the axis of the cylindrical sample. The slope of the ridge represents the longitudinal flow velocity of the fluid inside the rock. (C) Location of $t_\mu(\mathbf{r})$, determined as the center of the Gaussian distribution that was fitted to the dispersion curve of each voxel.

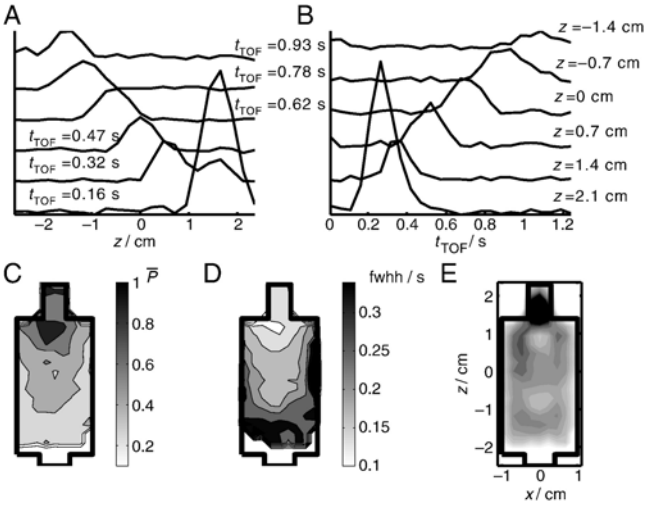

Fig. 2. Dispersion in a remote MRI experiment. The same data set as for Fig. 1 was used. (A) Combined effect of flow and dispersion on fluid displacement for different t_{TOF} values. The signal is shown as a function of encoding location along the axis of the cylindrical sample. The higher signal intensity for the curve with the shortest t_{TOF} is due to the higher porosity of the outlet volume compared with the rock sample. (B) Dispersion of the fluid for different encoding locations along the axis of the sample in the time domain. (C) Dispersion visualized as the maximum probability of finding fluid from a particular encoding location in the detector. (D) Dispersion visualized as the FWHH of TOF data, obtained by fitting a Gaussian distribution. (E) Effective porosity in a cross-section through the sample, showing two spots of reduced porosity on the axis.

When performing TOF experiments with spatially selective encoding, it is important that none of the encoded fluid passes the detector without being read out; otherwise, spin density gets weighted unevenly across the sample. The signal in a TOF experiment with imaging encoding, assuming the use of the abovementioned four-step phase cycle, can be described as:

$$S(\mathbf{r}, t_{TOF}) = \frac{S_0}{V_d} \int_{detector} d\mathbf{r}_d \int_{voxel} d\mathbf{r}' \, \rho(\mathbf{r}') P_S(\mathbf{r}_d, t_{TOF}|\mathbf{r}', 0). \quad (3)$$

S_0 is the signal per unit quantity of fully encoded spins, $\mathbf{r}$ denotes the center of a voxel inside the encoding coil (with $\mathbf{r}'$ being a volume element inside this voxel), $\mathbf{r}_d$ is a volume element inside the detector, ρ is the spin density of the fluid, t_{TOF} is the time between encoding and detection, and $P_S(\mathbf{r}_d,t_{TOF}|\mathbf{r}',0)$ is the conditional probability or propagator that a spin residing at $\mathbf{r}'$ during the encoding step (which is assumed to be negligibly short compared to t_{TOF}) is in the detector at time t_{TOF}. In this experiment, immobile fluid located in isolated pores does not contribute to the signal since it never reaches the detector.

Remote detection takes a purely Eulerian view of flow and dispersion [9]. One does not follow the displacement of spins from an initial location such as in the Lagrangian point of view, but spins are being tagged in one location and observed as they arrive at another predefined location in an external laboratory coordinate system. This strictly Eulerian view distinguishes this method from most of the established pulsed gradient spin-echo (PGSE) techniques to study flow and dispersion, and is the reason that the two techniques are largely complementary. Remote detection measures dispersion in a long-time limit, with the velocity of different fluid elements averaged out, thereby probing the influence of local variations of material properties on macroscopic fluid flow. PGSE methods, on the other hand, measure local displacement or velocity distributions directly, which allows one to draw statistical conclusions about the microscopic environment around fluid molecules.

Since remote detection characterizes the global flow field, Eq. (3) can be simplified using an averaged propagator

$$P(\mathbf{r}_d, t_{TOF}|\mathbf{r}, 0) = \frac{1}{N(\mathbf{r})} \int_{voxel} \rho(\mathbf{r}') P_S(\mathbf{r}_d, t_{TOF}|\mathbf{r}', 0) d\mathbf{r}', \quad (4)$$

where $N(\mathbf{r})$ is the number of spins in the voxel centered at $\mathbf{r}$. $P(\mathbf{r}_d,t_{TOF}|\mathbf{r},0)$ describes the probability of finding a spin originating within this voxel during encoding at $\mathbf{r}_d$ at a later time t_{TOF}. Equivalently, as long as detection is not performed in a spatially selective manner, the propagator can also be averaged over the active volume of the detector:

$$\bar{P}(\mathbf{r}, t_{TOF}) = \frac{1}{V_d} \int_{detector} P(\mathbf{r}_d, t_{TOF}|\mathbf{r}, 0) d\mathbf{r}_d. \quad (5)$$

Now, Eq. (3) can be rewritten as:

$$S(\mathbf{r}, t_{TOF}) = S_0 N(\mathbf{r}) \bar{P}(\mathbf{r}, t_{TOF}). \quad (6)$$

$\bar{P}(\mathbf{r},t_{TOF})$, the probability for the fluid encoded at voxel $\mathbf{r}$ to be in the detection volume at t_{TOF}, is the quantity that is directly accessible in the TOF dimension. If we make somewhat idealized assumptions that no fluid passes the detector without being read out, that all fluid passing the detector is being read out unweighted (i.e., the detector is equally sensitive across the whole detection volume and the signal is not influenced by some of the fluid being closer to the detector outlet when a detection pulse is applied) and that there is no correlation between encoding and detection location (complete mixing of the fluid at the outlet of the encoding volume), we can further analyze Eq. (6) using:

$$\sum_n \bar{P}\left(\mathbf{r}, t_{TOF}^{(n)}\right) = 1. \quad (7)$$

n indicates the nth step of a stroboscopic detection. The signal of this nth detection step depends on the fraction of the encoded fluid entering the detection volume subsequent to the $(n-1)$th step. In a nonideal experiment, the left-hand side of Eq. (7) may be smaller than 1 if not all the encoded fluid leaves through the detector within the detection time (e.g., if pores that are poorly connected to the flow field are present, which would require a disproportionately long detection time). Eq. (7) allows the separation of dispersion and spin density information, which is necessary to model

and interpret dispersion inside the porous medium. The simplest method used to visualize dispersion is a one-dimensional plot of $\bar{P}$ $(\mathbf{r},t_{\mathrm{TOF}})$ for selected voxels or for a specific t_{TOF}, as shown in Fig. 2A and B for dispersion along the spatial and time domains, respectively. One has to be careful when plotting dispersion in a two-dimensional plot since a broader dispersion pattern usually also means a lower maximum of $\bar{P}$ along t_{TOF}. Contour plots tend to suppress this broadening, as shown in Fig. 1B, while this representation works well in displaying fluid displacement.

To visualize more than one encoding dimension, parameters representing dispersion in a meaningful way are required, such as the full width at half height (FWHH) of $\bar{P}(t_{\mathrm{TOF}})$. For a symmetric dispersion pattern, the maximum of $\bar{P}(t_{\mathrm{TOF}})$ is related to the FWHH. As an example, Fig. 2C shows $\max(\bar{P}(\mathbf{r}))=\max(S(\mathbf{r},t_{\mathrm{TOF}}))/\sum_n S(\mathbf{r},t_{\mathrm{TOF}}^{(n)})$, and Fig. 2D shows the FWHH of $\bar{P}(\mathbf{r},t_{\mathrm{TOF}})$ of gas flow through the rock. The two patterns are similar, indicating that the dispersion is relatively symmetric around its maximum.

The effective porosity ϕ_{e}, the volume fraction of the pore space that is fully interconnected and contributes to fluid flow, is a parameter often used to characterize flow in porous media [5,10]. By assuming that the spin density in fluid-filled pores is uniform, knowledge of $N(\mathbf{r})$ can be used to determine ϕ_{e}. Since remote detection only registers fluid that leaves the medium within the total detection time, the localized effective porosity $\phi_{\mathrm{e}}(\mathbf{r})$ is proportional to the voxel-averaged spin density of the mobile fluid:

$$\tilde{\rho}(\mathbf{r}) = \frac{1}{V_{\mathrm{v}}}\int_{\mathrm{voxel}} \rho(\mathbf{r}')\,\mathrm{d}\mathbf{r}' = \frac{N(\mathbf{r})}{V_{\mathrm{v}}} \approx \frac{\sum_n S\left(\mathbf{r},t_{\mathrm{TOF}}^{(n)}\right)}{S_0 V_{\mathrm{v}}}. \tag{8}$$

V_{v} is the volume of an encoded voxel. For the rock example, $\rho(\mathbf{r})$ is shown in Fig. 2E. Effective porosity can be obtained as $\phi_{\mathrm{e}}(\mathbf{r})=\tilde{\rho}(\mathbf{r})/\rho_0$, with ρ_0 being the bulk spin density of the fluid.

A different definition of effective porosity links the specific discharge $q=Q/A$ with the mean velocity $v(\mathbf{r})$ of the fluid along the flow direction:

$$\phi_{\mathrm{e}}(\mathbf{r}) = \frac{q}{v(\mathbf{r})}. \tag{9}$$

Q is the volumetric fluid flow rate and A is the cross-sectional area of the porous sample. $v(\mathbf{r})$ can be determined in a TOF experiment from the distance Δz between two neighboring voxels along the flow direction, divided by the difference of the TOF between the two locations (Fig. 1B). The simplest way to determine this TOF value is to use the position of the maximum of the dispersion pattern $t_{\mu}(\mathbf{r})$, which is accurate if the dispersion pattern in the time domain is symmetric. Plotting $t_{\mu}(\mathbf{r})$ gives a qualitative estimate of the homogeneity of flow in the porous medium (Fig. 1C).

All examples were obtained from one data set, illustrating the rich information content in experiments with three-dimensional phase encoding and TOF detection. These experiments are ideal for use in characterizing fluid flow in porous media. A more heterogeneous material may require a more refined model, but the same experimental data would still be sufficient to perform equivalent analyses.

Acknowledgment

The authors thank S. Han and J.A. Seeley for discussions and experimental assistance. This work was supported by the Director of the Office of Science, Office of Basic Energy Sciences, Materials Sciences and Nuclear Science Divisions, US Department of Energy under contract DE-AC03-76SF00098. E.H. was supported by a fellowship from the US Department of Homeland Security under DOE contract DE-AC05-00OR22750.

References

[1] Moulé AJ, Spence MM, Han S, Seeley JA, Pierce KL, Saxena SK, et al. Amplification of xenon NMR and MRI by remote detection. Proc Natl Acad Sci USA 2003;100:9122–7.
[2] Xu S, Yashchuk VV, Donaldson MH, Rochester SM, Budker D, Pines A. Magnetic resonance imaging with an optical atomic magnetometer. Proc Natl Acad Sci U S A 2006;103:12668–71.
[3] Raftery D, Long HW, Shykind D, Grandinetti PJ, Pines A. Multiple-pulse nuclear magnetic resonance of optically pumped xenon in a low magnetic field. Phys Rev A 1994;50:567–74.
[4] Granwehr J, Seeley JA. Sensitivity quantification of remote detection NMR and MRI. J Magn Reson 2006;179:280–9.
[5] Wang R, Mair RW, Rosen MS, Cory DG, Walsworth RL. Simultaneous measurement of rock permeability and effective porosity using laser-polarized noble gas NMR. Phys Rev E 2004;70:026312.
[6] Granwehr J, Harel E, Han S, Garcia S, Pines A, Sen PN, et al. Time-of-flight flow imaging using NMR remote detection. Phys Rev Lett 2005;95:075503.
[7] Harel E, Granwehr J, Seeley JA, Pines A. Multiphase imaging of gas flow in a nanoporous material using remote-detection NMR. Nat Mater 2006;5:321–7.
[8] Bear J. Dynamics of fluids in porous media. New York: American Elsevier; 1972.
[9] Seymour JD, Callaghan PT. Generalized approach to NMR analysis of flow and dispersion in porous media. AIChE J 1997;43:2096–111.
[10] Stephens DB, Hsu KC, Prieksat MA, Ankeny MD, Blandford N, Roth TL, et al. A comparison of estimated and calculated effective porosity. Hydrogeol J 1998;6:156–65.